Postprint of: Lipińska W., Ryl J., Ślepski P., Siuzdak K., Grochowska K., Exploring multi-step glucose oxidation kinetics at GOx-functionalized nanotextured gold surfaces with differential impedimetric technique, MEASUREMENT, Vol. 174 (2021), 109015
DOI: 10.1016/j.measurement.2021.109015

Exploring Multi-step Glucose Oxidation Kinetics at GOx-functionalized Nanotextured Gold Surfaces with Differential Impedimetric Technique

Wiktoria Lipińska[1], Jacek Ryl[2,3,*], Paweł Ślepski[2], Katarzyna Siuzdak[1] and Katarzyna Grochowska[1,*]

[1]Centre for Plasma and Laser Engineering, The Szewalski Institute of Fluid-Flow Machinery, Polish Academy of Sciences, Fiszera 14, 80-231 Gdańsk, Poland

[2]Department of Electrochemistry, Corrosion and Material Engineering, Gdańsk University of Technology, Narutowicza 11/12, 80-233 Gdańsk, Poland

[3]Advanced Materials Center, Gdańsk University of Technology, Narutowicza 11/12, 80-233 Gdańsk, Poland

Corresponding authors: Jacek Ryl: jacek.ryl@pg.edu.pl , phone/fax +48 583471092; Katarzyna Grochowska: kgrochowska@imp.gda.pl , phone +48 585225120

Abstract: For a few past years, we can observe the enormous growth of investigations related to ultrasensitive electrochemical sensors capable of reliable determination of important body parameters and analytes. Utilized procedures rely on standard electrochemical methods, demanding electrode polarization, and information about the initial characteristics of the working electrode. More and more complex electrode materials are characterized however their electrochemical response is not fully understood or defined, affecting data reproducibility.

Herein, we propose a novel protocol utilizing dynamic electrochemical impedance spectroscopy in galvanostatic mode (g-DEIS) to verify the sensor performance. The protocol was applied to study the response of Ti-Au nanotextured electrode depending on glucose concentration changes. The g-DEIS allowed to monitor complex mechanism occurring at the electrode/electrolyte interface with the continuously dosed glucose through electric parameters derivatives in analyte content. Our studies revealed a visible increase in electrode electric heterogeneity above 1.9 mM of glucose and gold nanoparticles' oxidation above 3.8 mM, both influencing electrode kinetics. The results were confirmed using supporting cyclic voltammetry and x-ray photoelectron spectroscopy studies. The proposed protocol's unique features could significantly spread further application of targetable biosensors for real-time diagnostics.

Keywords: g-DEIS, multisine impedance, electrode kinetics, glucose sensor, glucose oxidase, nanotextured Ti-Au

1. Introduction

In today's world, diabetes has become one of the major causes of death. The morbidity is spreading more and more every year due to the sedentary lifestyle and poor eating habits. Therefore, extensive research is conducted to ensure the frequent monitoring of glucose levels in human body fluids essential for maintaining this disease daily. Most glucose monitoring biosensors are electrochemical due to the low cost of production and reliability. The impedimetric sensors are not as thoroughly studied as potentiometric or amperometric ones; however, the Electrochemical Impedance Spectroscopy (EIS) allows exact measurements allows ultra-high sensitivity, ranging from 10^{-12} M glucose concentration [1,2]. Unfortunately, impedance spectroscopy's main drawback is that it is an indirect technique based on data fitting with adequate models, which typically require full knowledge regarding the studied system's initial electric state.

Electrochemical sensors detect differences in the charge transfer due to the analyte interaction with specifically functionalized electrode surface [3–5]. The initial electrode conditions are never fully known. Subtle, yet uncontrollable differences in the functionalization film thickness or surface homogeneity may introduce an alteration in the charge transfer kinetics, which is a significant threat for results reproducibility. This threat is partially minimized by standardization of the electrode pre-treatment processes and determination of the electrode's response prior to its utilization as the biosensor. Knowing that the charge transfer kinetics are dependent on glucose concentration, one has to consider the differentiated electrochemical response in modeling the impedance data and building the calibration curve.

The protocol utilizing Dynamic Electrochemical Impedance Spectroscopy (DEIS) allows to resolve some level of uncertainty related to variable electrode kinetics, allowing the monitoring of capacitance dispersion degree and thus local inhomogeneity of the electrode material. The theoretical background for the DEIS technique was proposed by Darowicki [6]. The goal was to handle the impedance measurements of the non-stationary corrosion processes. Slepski undertook the construction of the first operating measuring tool shortly after [7]. The assumption of DEIS measurements is to abandon the frequency response analyzer (FRA) sequential perturbation in favor of a multi-frequency sinusoidal signal package, continuously applied to the investigated system throughout the measurement duration. Individual sinusoids are characterized by adequately selected and optimized values of frequencies, amplitudes, and

phase shifts. Simultaneously, the analyzed frequencies' scope is limited to ~1 Hz, which restricts each impedance spectrum acquisition time. The so-called window function cuts out fragments of the recorded response signal, decomposed using Fourier transform. This procedure allows limiting the acquisition time of a single impedance spectrum down to even 1 second. The acquisition time depends entirely on the window function's size, which depends on the lowest measured frequency of the perturbation signal. Such an approach ensures meeting the *quasi*-stationary conditions and allows to investigate a significant number of real systems. Throughout the last decade, the technique has gained considerable attention. It was used in numerous studies related not only to corrosion processes [8–12], but also to energy conversion [13–15], chemical-mechanical failure [16,17], impedance mapping [18–20], electropolymerization [21–23], or adsorption phenomena [24,25].

One should also pay attention to the studies of Bandarenka et al. [26–28], taking into consideration the high analytical importance of capacitance dispersion due to surface heterogeneity and tracking impedance changes during electrochemical oxidation/reduction processes. DEIS carried out in potentiodynamic mode allows observing subtle structural modifications at the interface between the platinum electrode and the electrolyte. These modifications were related to surface transformation occurring in the two-dimensional adsorption layer, which was explained by a relatively slow exchange of ions between the outer and inner Helmholtz plane. For example, studies of oxygen electroreduction on Pt allowed for the isolation of three free radical intermediates at the electrode surface [26]. The utilization of potentiodynamic DEIS measurements has its first implementation in biosensing. The technique allowed for the detection of DNA hybridization by tracking the capacitance dispersion effects of the specifically-anchored oligonucleotide sequences at the anodically polarized boron-doped diamond electrode interface [4].

Due to the impossibility of an unambiguous determination of the initial electrode conditions, the differential analysis of the instantaneous changes of measured parameter emerges as a possibly lucrative approach towards sensory application. An analogous procedure was successfully applied in monitoring resonating frequency [27,28], electrochemical or acoustic noise [9,29], optical indices [30,31], etc. In electrochemical studies, the system's instantaneous monitoring is possible due to dynamic impedance measurements in galvanostatic mode (g-DEIS), controlling the charge flowing through the electrode. This mode of operation in multisinusoidal impedance measurements was proposed first by Slepski and Ryl to handle the appearance of undesired polarization of the working electrode introduced by changes of the open circuit potential (OCP) [15,32,33]. Ryl and Wysocka adopted g-DEIS methodology in

their studies focused on efficient adsorption isotherm determination, carried out during controlled corrosion inhibitor injection to the electrolyte during the measurement [24,25].

As the goal of this work, we explore the mechanism of glucose influence on GOx-anchored over gold nanoparticles (AuNPs) based electrode using differential g-DEIS impedance analysis, revealing the complex adsorption mechanism and charge-transfer interactions. We have chosen modified Au nanostructures integrated with textured Ti platform as the investigation object since both gold and titanium are regarded as biocompatible materials ensuring direct contact with the human body that is of high importance for further real application in glucose diagnostics [34]. The composition of the electrode has been already optimized and characterized using microscopy and standard electrochemical methods while its sensing parameters have been already compared with others [35]. On the contrary to our previous work, herein the applied protocol boosts the high applicability of g-DEIS monitoring to measure the electric parameters' derivative as a function of time and glucose concentration, independent of the electrode boundary conditions and heterogeneity, providing essential information on changes of biosensor kinetics. Similar studies have not been reported before and could state as a valuable support for other sensor-like investigations to the best of our knowledge.

2. Experimental

2.1. Ti-Au nanotextured electrode fabrication

The investigated electrode material is composed of a dimpled Ti plate where each cavity is filled with a single gold nanoparticle and modified with glucose oxidase. The composite structure was prepared via a three-step procedure covering a) fabrication of TiO_2 nanotubes accompanied (TiO_2NTs) with their subsequent etching, b) formation of AuNPs, and c) GOx immobilization.

Before anodization, rectangular Ti plates (2×3 cm^2, Strem 99.7%) were degreased in acetone, ethanol, and deionized water for 10 min in each medium, respectively. Afterward, each Ti plate was used as an anode and Pt mesh as a cathode in a two-electrode arrangement. Both electrodes placed opposite to each other were immersed in the cylindrical glass reactor filled with organic-water electrolyte. The synthesis protocol covers two subsequent anodization stages, followed by the etching of as-grown titania nanotubes. For each anodization batch, the electrolyte was composed of 0.27 M NH_4F dissolved in 99%/1% vol/vol ethylene glycol/water mixture. To grow the TiO_2NTs layer the voltage of 40 V was kept for 2 h and 6 h for the first

and the second anodization stage while the temperature of 23°C was maintained. The rate of voltage increase and the decrease was set to be 0.1 V/s and controlled by dedicated software. The TiO_2NTs removal performed after the 1st and 2nd anodization was realized via overnight immersion in diluted 0.5% oxalic acid. After the second etching procedure, the Ti substrate was rinsed in ethanol and dried. Such material ascribed as titanium nanodimpled foil (TiND) was used for the next step of the fabrication procedure. The synthesis of gold nanoparticles starts from the evaporation of 10-nm thin Au film using magnetron sputtering machine (Q150T S system, Quorum Technologies) where the thickness of the formed metal coating is controlled by quartz crystal microbalance. Afterward, substrates were loaded in the electric oven for 10 min at 450°C to ensure rapid thermal treatment. The obtained material was labeled as Au-TiND. Then, the modification by glucose oxidase was performed. The procedure was based on the approaches proposed by Crespilho et al. [36] and Li et al. [37] and modification exhibits cross-linking character. The mixture used for the modification contains 4 mg bovine serum albumin (BSA, Serva), 2.5% glutaraldehyde (GA, Sigma Aldrich) and 0.5 mg/mL of GOx (135200 units/g, Sigma Aldrich from *Aspergillus niger*). The BSA/GA/GOx solution was dropped onto the Au-TiND substrate and stored for 2 h in ambient conditions. When the incubation time has passed, the surface was washed by 0.1 M PBS, and then the sample (GOx/Au-TiND) was kept at 4°C until the electrochemical measurements. The whole modification process regarding enzyme anchoring was described in details in our previous work [35].

2.2.Ti-Au nanotextured electrode characterization

The material's surface topography at each fabrication step was verified using scanning electron (SEM) and atomic force (AFM) microscopies. SEM images for substrates at each fabrication step were captured using FEI Quanta FEG250 equipped with ET secondary detector, with 20 kV accelerating voltage. The AFM profile for dimpled TiND substrate was recorded using Nanosurf EasyScan2 in the contact mode regime.

The Dynamic Electrochemical Impedance Spectroscopy in galvanostatic mode (g-DEIS) studies were performed on functionalized GOx/Au-TiND electrode during glucose injection to 0.1 M PBS electrolyte (pH=7.4). The initial OCP value was -0.09 ± 0.02 V vs. $Ag|Ag_2O$. The microflow peristaltic pump (Fluid BQ80S, China) was set to dose glucose to the electrochemical cell at a constant flow rate of 10 μL/min after an initial conditioning period of GOx/Au-TiND electrode in 0.1 M PBS. The injection was conducted upon reaching 10 mM of glucose in the electrochemical cell, which lasted for four hours. The g-DEIS studies were

carried out at zero DC current, which corresponds to OCP conditions. A linear increase of the OCP by 40 mV was recorded with glucose injection.

The three-electrode assembly was used, where: GOx/Au-TiND was the working electrode (WE), $Ag|Ag_2O$ served as a reference electrode (RE), and the Pt mesh as a counter electrode (CE). The g-DEIS measurement setup consists of Autolab PGSTAT 302N (Metrohm, Netherlands) galvanostat and two measurement cards: PXI-4464 for the generation of AC signal and PXI-6124 for the acquisition of AC/DC signals (both from National Instruments, USA). The g-DEIS measurements were carried out using a multisinusoidal perturbation signal composed of 29 elementary signals of various frequencies between 4.5 kHz and 0.3 Hz, with 7.5 points per decade frequency. The amplitude of the perturbation signal was controlled to assure that the response signal amplitude does not exceed 20 mV. The analytical window length was 10 s.

Four GOx/Au-TiND electrodes were tested by cyclic voltammetry (CV) using: potentiostat/galvanostat AutoLab PGStat 302N (Metrohm, Netherlands). The three-electrode system was used: GOx/Au-TiND as WE, Ag/AgCl/0.1M KCl as RE, and Pt mesh as CE. The air-saturated 0.1 M PBS was the supporting electrolyte with different amounts of glucose in the range of 0-10 mM. The CV scanning rate was 50 mV/s. Fifty polarization cycles were conducted for each electrode, from -0.5 V to +1.3 V. The amount of cycles ensured Au oxidation on the whole electrode surface and prevented the degradation of the modification.

The X-ray photoelectron spectroscopy (XPS) measurements were performed using Escalab 250Xi spectroscope (ThermoFisher Scientific), with a monochromatic AlKα source. The high-resolution spectra of *Au4f* for GOx-functionalized electrodes were showed. Calibration based on Au metal (84.0 eV).

3. Results and discussion

As a model electrode material within this work, we propose the dimpled titanium foil (TiND) covered with Au nanoparticles (Au-TiND) and functionalized with glucose oxidase (GOx/Au-TiND). This particular electrode material arrangement has been already optimized using different anchoring approaches and GOx content in the batch while depending on the applied electrochemical technique (cyclic voltammetry, differential pulsed voltammetry) the sensing parameters were compared to the literature data [35].

Following the Experimental section's description, each step of the fabrication procedure of the Au-TiND electrode material results in different morphology as depicted in **Fig. 1**. Highly ordered aligned titanium dioxide nanotubes are received after the second anodization stage onto the initially used flat Ti substrate. Their length reaches ca. 2.8 μm, whereas the internal diameter and the wall thickness equal to 85 nm and 15 nm, respectively (see **Fig. 1a**). The overnight immersion in oxalic acid solution resulted in the complete removal of TiO_2NTs and textured Ti foil remains. As shown in **Fig. 1b**, the topography stays as a perfect imprint of the bottom part of the TiO_2NTs layer showing uniformly distributed cavities adhering to each other [38,39]. According to AFM profile (see inset in **Fig. 1b**), each cavity has a ca. 85 nm diameter, whereas its depth reaches 6.9 nm. The dimples dimensions were determined as an average value of 30 measurements at different places of the sample. After Au deposition, the initially sharp edges between cavities became smoother (**Fig. 1c**). Further thermal annealing results in each dimple's occupation by a single gold nanoparticle (**Fig. 1d**). The obtained substrate is used as a nanostructured platform for modification with GOx. Following that, the proposed procedure could be regarded as a relatively simple one, allowing fabrication of the electrode material exhibiting a very high degree of ordering over the sizeable geometric surface area that is of significant importance considering sensor application. Nevertheless, the microscale's surface complexity is relatively high and should be considered during electrochemical studies.

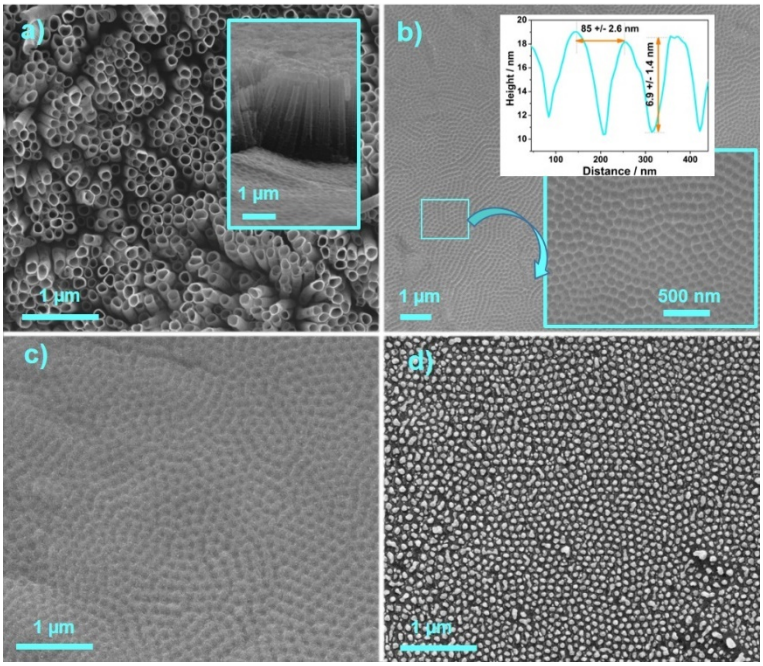

Fig. 1. SEM image of a) TiO_2 nanotubes (inset: cross-section image of TiO_2NTs), b) titanium nanodimples (inset: AFM profile), c) TiND covered by thin Au layer, d) TiND substrate filled with AuNPs.

The Dynamic Electrochemical Impedance Spectroscopy in galvanostatic mode was carried out at zero DC current ($i_{DC} = 0$) to reflect the open circuit potential conditions. A total of 1440 independent impedance spectra were recorded at the end of each experiment resulting from the length of the analytical window function (10 s). The exemplary instantaneous impedance spectra obtained throughout the glucose injection measurement are shown in **Fig. 2a.** The impedance spectra reveal slight changes in the analyzed system's electrochemical response, easier to recognize in classic 2D projection. Thus, **Fig. 2b** shows the capacitance impedance spectra in the Nyquist projection at selected time points representative for glucose concentration of 1, 2, 4, 6, 8, and 10 mM, transformed according to the procedure proposed elsewhere [40,41].

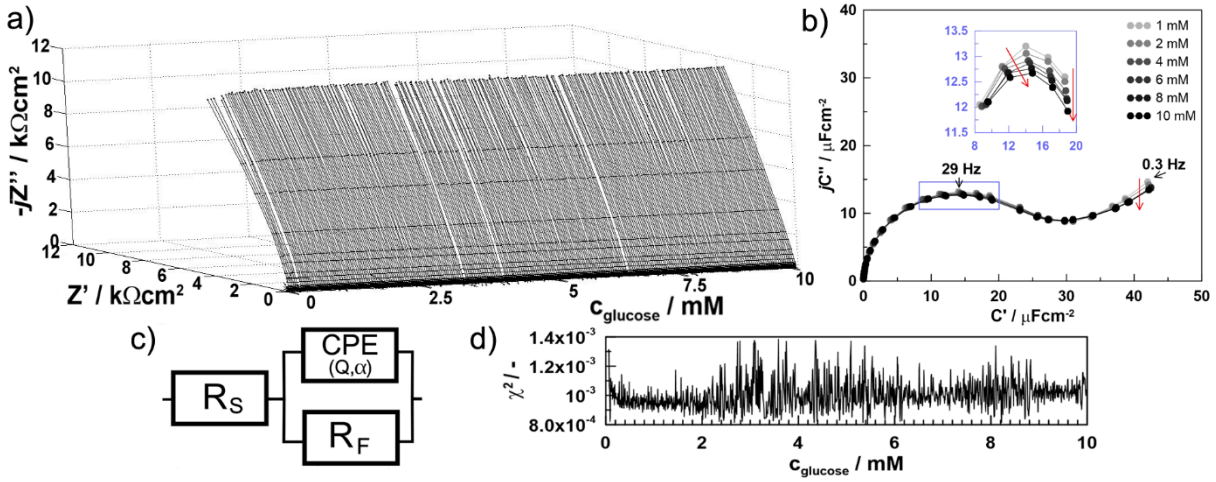

Fig. 2. a) g-DEIS impedance spectra in the Nyquist plot, registered during the experiment with changes of the injected glucose concentration on the X-axis; b) exemplary spectra obtained throughout the measurement, plotted in the form of capacitance Nyquist plot; c) $R_S(CPER_F)$ EEC used for spectral analysis; d) χ^2-distribution for selected EEC.

Each impedance spectra is built of a single, dispersed time-constant. Over time, the increase of glucose concentration leads to a slight but consistent decrease of capacitance on the electrode/electrolyte interface, marked with red arrows. A more detailed analysis is possible after the selection of the electric equivalent circuit (EEC) to fit the impedance data. Based on the shape of obtained spectra and previous literature findings [42–44] we proposed a modified Randles circuit. The R_S(CPE-R_F) EEC consists of electrolyte resistance R_S, GOx-functionalized film resistance R_F and constant phase element CPE, schematically presented in **Fig. 2c**. The

constant phase element represents the capacitive behavior of functionalized film and its heterogeneity. Its impedance is given with eq. (1):

$$Z_{CPE} = [Q(j\omega)^{\alpha}]^{-1} \quad (1)$$

It should be noted that in the boundary case, if α=1, the CPE impedance responds to the capacitor of capacitance Q. In contrast, for α=0, the CPE impedance is assigned to the resistor of resistance 1/Q. Therefore CPE exponent α is often considered as the homogeneity factor; its decrease corresponds to the increase of heterogeneity, while Q reflects the *quasi*-capacitance of the heterogeneous electrode interface.

The *quasi*-capacitance describes the complex charge accumulation at the heterogeneous, functionalized GOx/Au-TiND electrode surface. Its changes may originate from the change in electrode electric homogeneity through eq. (1), and the actual changes in the double layer capacitance or functionalized film capacitance, as defined with eq. (2).

$$C = \frac{\varepsilon_0 \varepsilon A}{d} \quad (2)$$

Here, ε_0 and ε refer to vacuum permittivity and relative permittivity of GOx-functionalized electrode interface, respectively, A is the electrochemically-active electrode surface area and d stands for the functionalized layer thickness. Homogeneity factor α influence standardization requires estimation of the effective functionalized film capacitance C_{EFF} with one of the available algorithms [45]. Eq. (3) defines C_{EFF} in the case of the surface distribution of the time constants.

$$C_{EFF} = Q^{1/\alpha}(R_S^{-1} + R_F^{-1})^{(\alpha-1)/\alpha} \quad (3)$$

The impedance spectra were analyzed using the Nelder Mead algorithm. The selected EEC offered high fitting quality, represented by the χ^2-distribution, see **Fig. 2d**. The lowest fit quality was found in the concentration range between 2 and 6 mM, possibly originating from higher system non-stationarity at that time, yet it did not exceed 1.4×10^{-3}. It should be noted that χ^2-distribution should not be considered the primary factor during EEC selection, as illustrated by the example present in the **Supplementary Information file, section S1**.

The absence of additional time constants in the EEC originates from two factors: similar relaxation times of the occurring processes and the g-DEIS restriction regarding the low-frequency measurement range. The lowest applied frequency is constrained by the length of the analytical window, which, on the other hand, is constrained by the non-stationary behavior of the investigated system [8,23]. More developed EEC models were also evaluated during the

impedance data analysis and discussed in **Supplementary Information Figs. S1, S2**. Here, another significant advantage of g-DEIS measurements emerges in comparison to the classic EIS approach. The single numerical values most often provided with EIS studies do not allow for a direct verification if changes of the EEC parameters are physically explicable. Lack of continuity of analyzed electric parameters disqualifies their selection.

Fig. 3 presents the scheme of g-DEIS impedimetric measurement methodology, which consists of two parallel experiments, without and with glucose injection, as shown in **Fig. 3a**. The recorded instantaneous impedance spectra are fitted with EEC to obtain the electric parameters (see **Fig. 3b**).

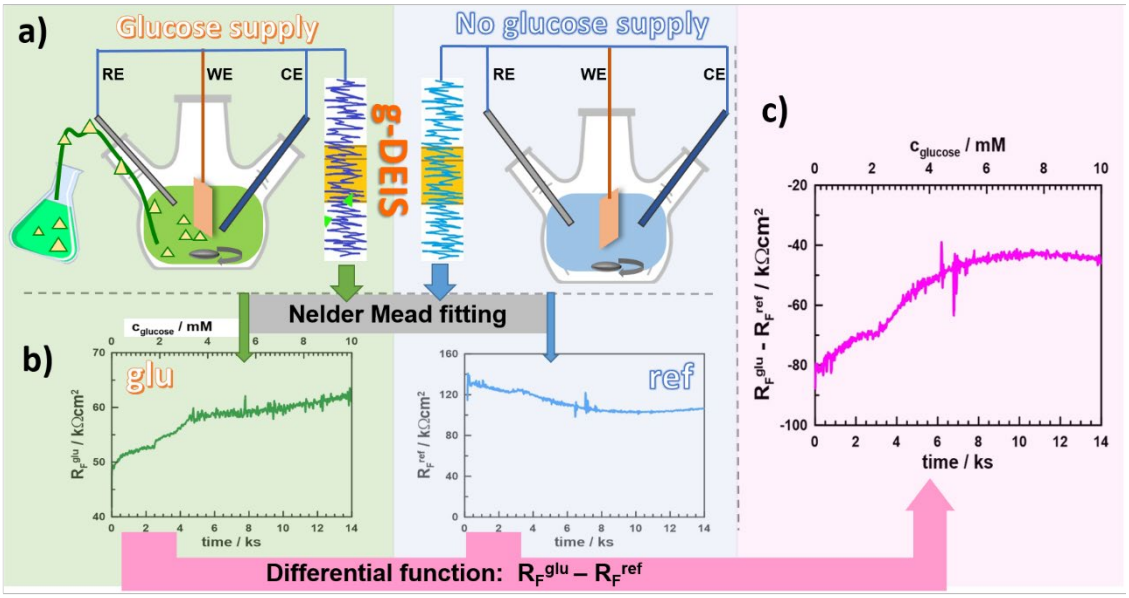

Fig. 3. a) Schematic representation of the electrochemical setups: left - with glucose supplied by a peristaltic pump, right – used for the reference experiment. b) The fitting process's output with the Nelder Mead algorithm while resultant electric parameters were used further in differential function leading to graph c).

The complex changes of the impedance parameters are dependent on (i) the initial electrode conditions and (ii) environmental factors affecting the investigated system. The studied electrode's initial electric parameters are influenced mainly by uncontrollable differences in bulky enzyme-functionalized layer thickness, subtle variation in electrode geometry, and electroactive surface area. Even small changes in electrode or electrolyte parameters will alter experimental conditions. Therefore, the protocol based on differential impedance analysis leading to the final output graph given in **Fig. 3c** emerges as the new possible approach to evaluating complex electrode kinetics.

The differential impedimetric analysis of the studied electric parameters: R_F, C_{EFF}, Q, and α are shown in **Fig. 4**. The oxygen is the primary factor affecting electrode response in glucose absence through direct interaction with the enzyme or the corrosion process in Au-TiND nano-galvanic cells. The second set of measurements was done after purging the electrolyte with argon to evaluate the oxygen influence on the studied system.

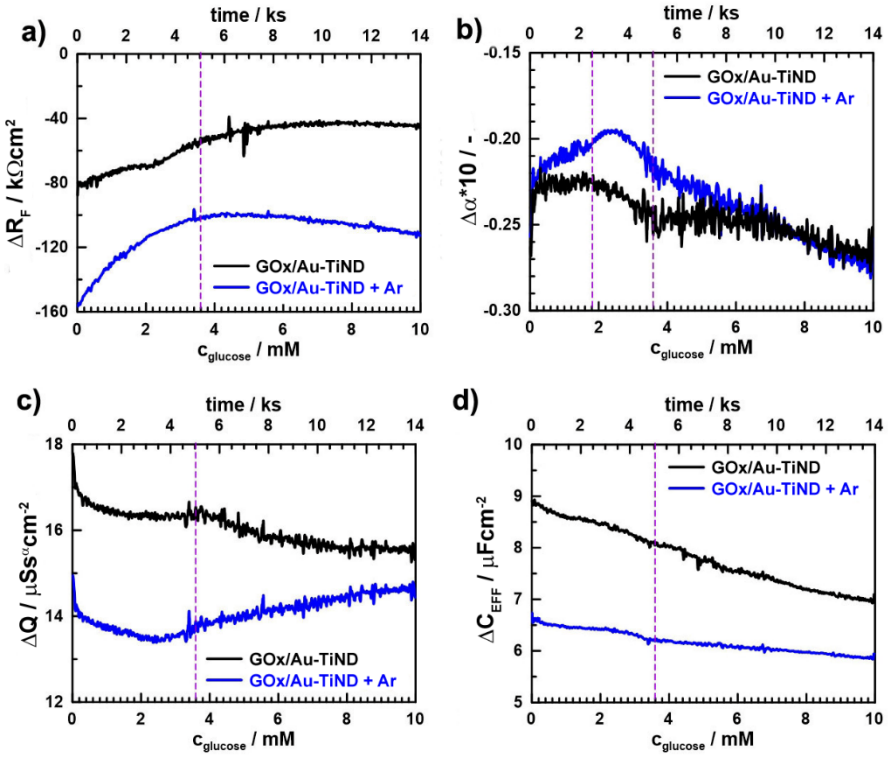

Fig. 4. Instantaneous changes of: a) enzyme-functionalized film resistance R_F; b) CPE exponent – the homogeneity factor α, and c) CPE *quasi*-capacitance Q; d) functionalized film effective capacitance C_{EFF}.

The observed changes in the functionalized film resistance present quite complex behavior. The ΔR_F parameter value (**Fig. 4a**) initially increases but reaches a plateau later on. This behavior is independent of argon purging; however, in the absence of dissolved oxygen, the measured resistance values are slightly higher, possibly due to the oxygen depolarization process occurring at the Au-TiND electrode interface.

Neither of the reference experiments (with or without argon purging) was characterized by an increase in R_F over experiment duration, which confirms that glucose injection is directly responsible for successful inhibition of the charge transfer through the enzyme-functionalized film at the electrode surface. The above could be assigned to the interaction between glucose and GOx-functionalized Au-TiND electrode, according to eqs. (4-6) [46]:

$$\text{Glucose} + \text{GOx(FAD)} \rightarrow \text{Gluconic acid} + \text{GOx(FADH}_2\text{)} \quad (4)$$

$$\text{GOx(FADH}_2\text{)} + \text{O}_2 \rightarrow \text{GOx(FAD)} + \text{H}_2\text{O}_2 \quad (5)$$

$$\text{H}_2\text{O}_2 \rightarrow \text{O}_2 + 2\text{H}^+ + 2\text{e}^- \quad (6)$$

Following eq. (4) enzyme FAD centers present on the electrode surface start to saturate, restricting the electrochemically active surface area. The function $\Delta R_F(c_{glucose})$ is characterized by inflection at $c_{glucose}$ = 3.8 mM. The most likely explanation for the alteration of charge transfer kinetics at that concentration is the appearance of secondary electrode processes at that point. It should be noted that the following trend of changes is possible either due to (i) the occurrence of two competitive processes at low glucose concentrations, one of which is ceased at some point, or (ii) initiation of the electron transfer reaction at higher concentrations. The authors' hypothesis favors the second option. Initiation of a redox process results in the drop of functionalized film resistance through the electrode, an observation widely reported in previous DEIS studies [7,40,47]. In authors' opinion, metallic gold oxidation in the presence of H_2O_2 is responsible for the observed change in charge transfer kinetics. Being the product of eq. (5), H_2O_2 could release the oxygen according to eq. (6). The hypothesis will be evoked further on. On the other hand, full and uniform blockade of GOx-functionalized electrode by glucose molecules takes place at glucose concentrations exceeding 10 mM.

More detailed information regarding the glucose influence may be obtained by studying the parallel capacitance changes. As mentioned before, the CPE exponent α is considered the electrode homogeneity factor. The $\Delta\alpha$ changes are presented in **Fig. 4b**. The electric homogeneity of the studied electrode is not strongly affected at the start of the experiment. However, after reaching approx. 1.9 mM glucose concentration, the value of α is slowly decreasing. This feature is negligibly affected by the oxygen content; however, if argon is purged into the system before the experiment, the electrode homogeneity is higher.

The most prominent influence on electrode homogeneity is visible after exceeding a glucose concentration of 3.8 mM. This observation is in good agreement with the proposed electrode blockade mechanism. The injected glucose adsorbs at the electrode surface interacting with GOx at the most outer layers of functionalized Au-TiND substrate. Consequently, it leads to the local modification of the charge transfer kinetics through the appearance of temporarily saturated areas within the enzyme-anchored platform [48]. The higher the glucose concentration, the deeper the enzyme layers are affected. Negligible $\Delta\alpha$ changes observed in the initial period of the experiment reflect the behavior of partially-blocked, spatially heterogeneous electrodes with small-sized blocked areas. Davies and Compton thoroughly

investigated the following subject when considering the distribution of the diffusion layers for electrodes composed of conductive and insulating parts [49–51]. However, in our case, the electrochemically heterogeneous surface is less defined since the local dispersion is characterized by less evident differences in conductivity. The conductive areas' local dispersion is initiated with larger enzyme saturated areas and blocked zones within the functionalized film.

While the *quasi*-capacitance Q alone does not provide valuable information without its proper standardization to C_{EFF}, the ΔQ was plotted in **Fig. 4c** for comparison. Next, the ΔC_{EFF} function obtained through eq. (3) is plotted in **Fig. 4d**. When comparing the obtained results with and without argon purging, one can see a significant difference in the electrode characteristics introduced by glucose injection. Interestingly, in both studied cases, the resultant effective capacitance changes reveal a nearly-linear decrease with linearly growing glucose concentration. GOx-functionalized film blocks the charge transfer on glucose injection, gradually restricting the electroactive surface area, decreasing the effective capacitance. Furthermore, as was reported by Liao et al. [52], the relative permittivity of aqueous glucose solution decreases with the increase of glucose concentration in a linear manner. Both of these relationships explain the linear fall of the C_{EFF} value during glucose injection. However, when the amount of oxygen is minimal, the ΔC_{EFF} parameter is significantly less affected. Carrying out the experiment without glucose dosing or purging electrolyte with argon, the C_{EFF} parameter slowly and linearly increases (approx. by 1 μF), assigned to the corrosion process occurring in nanogalvanic Au-TiND cells.

The voltammetry tests were also performed in 0.1 M PBS to confirm the sensing capability of the GOx-functionalized electrode and validate the concentration range of its performance, plotted in **Fig. 5a**. The little oxidation hump was observed at +0.9 V in the pure PBS solution, whereas at the reverse scan the reduction at ca. +0.4 vs. Ag/AgCl/0.1M KCl was recorded. Those signals are attributed to the gold oxide formation and its further reduction, respectively [53]. Systematic growth of the oxidation current density at +0.9 V vs. Ag/AgCl/0.1M KCl occurs along with the increase of glucose level, as shown in **Fig. 5a**. Three ranges exhibiting different slopes emerge regarding the tendency of current change. The most rapid change is found in the lowest glucose concentration range, up to 2 mM, while above it, the current growth rate noticeably changes its dependence. The sensitivity values in those linear ranges equal to 19.3 and 23.9 μA cm^{-2} mM^{-1} for the lowest (in green frame, **Fig. 5a**) and medium (in yellow frame, **Fig. 5a**) glucose level, respectively.

Upon further glucose dosage (shown in the blue frame, **Fig. 5a**), when the concentration exceeds 4 mM, the slope diminishes, and the current density reaches the plateau near 10 mM. It can be then concluded that for concentrations above 10 mM the enzyme active centers are filled with glucose. However, we would like to underline that from the application point of view, the sensitivity value (4.8 µA cm^{-2} mM^{-1}) found in the highest glucose level (blue frame in **Fig. 5a**) cannot be considered for reliable detection.

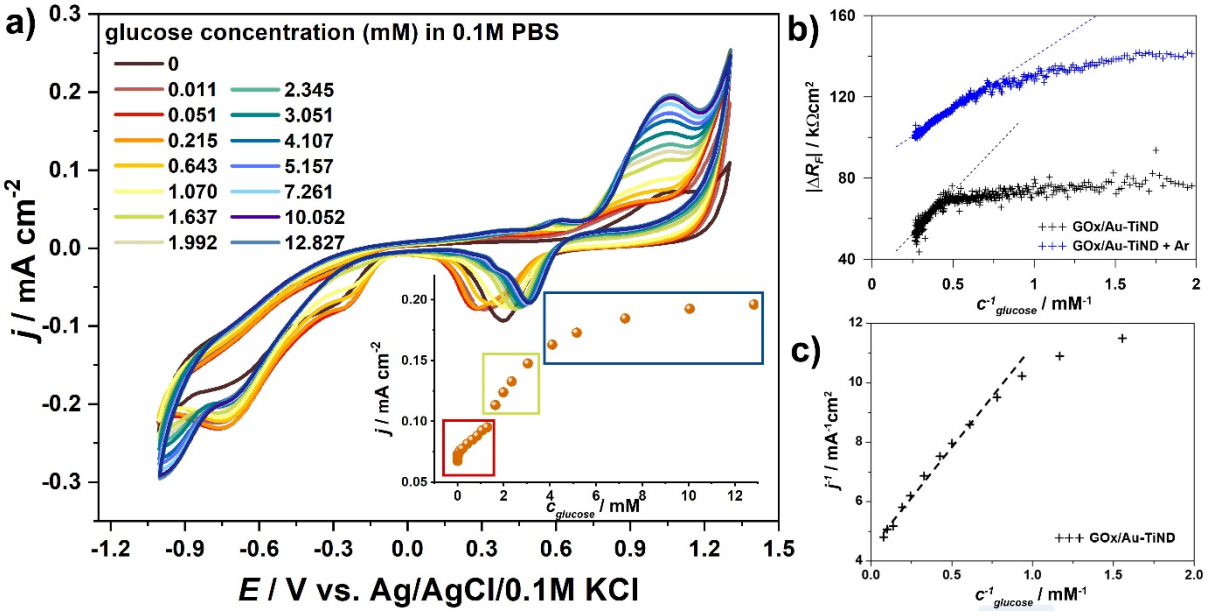

Fig. 5. a) CV curves registered for GOx/Au-TiND electrode in the air-saturated 0.1 M PBS for different glucose concentrations; b-c) the Lineweaver-Burk plot of the GOx/Au-TiND biosensor, based on: b) dynamic impedance response, c) voltammetric response.

While the CV allows evaluating glucose oxidase based on gold oxidation, through the polarization peak at +0.9 V, the analogous g-DEIS results hint at the possibility of Au oxidation already at OCP conditions. The activity of glucose oxidase is directly dependent on oxygen and glucose availability. The GOx catalyzes glucose oxidation to gluconolactone and H_2O_2 using oxygen, while gluconolactone is hydrolyzed to gluconic acid. The process was tracked with the titrimetric method; chromogenic substrate color changes were monitored spectrophotometrically [54,55]. According to the complementary interpretation proposed by [56,57], a summary reaction eq. (7) is likely to occur.

$$4Au + 4H_2O_2 \rightarrow 2Au_2O_3 + O_2 + 8H^+ + 8e^- \quad (7)$$

The Michalis-Menten constant (K_M) was estimated for the studied system based on both g-DEIS and CV measurements, to determine the biological activity of the immobilized enzyme.

This parameter is derived from the Lineweaver-Burg equation based on voltammetric response using eq. (8) [58,59].

$$\frac{1}{i_{SS}} = \frac{K_M}{i_{max}} \frac{1}{c_{glucose}} + \frac{1}{i_{max}} \quad (8)$$

where i_{SS} and i_{max} are currents measured for glucose detection under steady-state and GOx saturation, respectively. Similar estimation may be drawn from g-DEIS results, based on ΔR_F function, given into consideration that at low overpotentials eq. (9), is met.

$$R_F = B\frac{1}{i} \quad (9)$$

where B is the proportionality constant. More detailed information is given in the **Supplementary Information file, section S2**. The GOx enzyme kinetic constant, K_M, was found to be equal to 2.45 mM when estimated based on the g-DEIS data (**Fig. 5b**) and 1.54 mM based on the CV results (**Fig. 5c**). The difference derives from different analytical approaches and electrode polarization ranges. The K_M values reported for the enzymatic glucose sensors containing AuNPs show large discrepancies: from 0.23 mM [60], 0.6 mM [48], 1.08 mM [58] and even 5.66 mM [59]. Here, both the obtained results match the literature survey. Importantly, performing the electrochemical measurement under argon purging reduces the K_M value obtained with g-DEIS technique, down to 0.6 mM. The above suggests that glucose interaction is prone to interference by oxygen concentration through eq. (5) and (6), a problem wider described elsewhere [61]. Moreover, a smaller K_M value indicates higher enzyme activity and affinity to glucose. This phenomenon was observed and discussed by Asrami et al. [62], who suggested that the atmospheric oxygen molecules dissolved in the electrolyte adsorb at the sensor surface, forming a semiconducting film (TiO_2 in this case). As a consequence, the decrease of the transducer conductance is observed, hindering the electrochemical glucose oxidation step represented with eq. (6).

The high-resolution X-Ray Photoelectron Spectroscopy (XPS) studies were carried out on GOx-functionalized Au-TiND electrode to verify the possibility of gold oxidation at OCP conditions and the hypothesis regarding the role of H_2O_2 at the third observed phase of glucose interaction. These measurements were carried out for the electrodes pre-exposed in the electrolyte with specific glucose concentration. The measurements were carried out in *Au 4f* binding energy (BE) range at glucose concentrations of 1, 3, 6, and 10 mM. **Fig. 6a** reveals the Au4f XPS spectra' shape at the lowest and the highest analyzed glucose concentration.

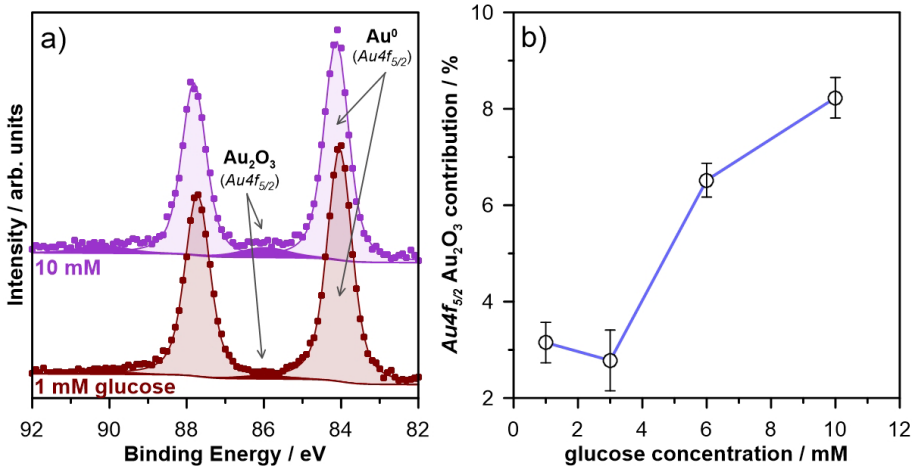

Fig. 6. High-resolution XPS spectra recorded at *Au4f* BE range with proposed peak deconvolution, and b) the changes of *Au* $4f_{5/2}$ Au_2O_3/$Au(OH)_3$ component share in the total signal from gold.

The deconvolution model was composed of two peak doublets. First, the dominant component with *Au* $4f_{5/2}$ peak located at BE of 84.0 eV should be ascribed to the metallic gold [63–65]; however, the model was enriched by the second peak doublet with *Au*$4f_{5/2}$ peak at 85.8 eV. While its absence during data analysis for the lowest glucose concentration does not lead to significant fitting errors, the secondary component's peak area gradually increases and is non-negligible at higher concentrations. This peak doublet is most often ascribed to Au(III) [66,67], confirming the presence of gold oxides and/or hydroxides.

The Au(III) share in the total [Au] signal recorded was plotted versus glucose concentration in **Fig. 6b**. This data reveals that gold electrode substrate undergoes gradual oxidation, most likely under mechanism proposed in eq. (7). The oxidation process is restricted to exposure at electrolytes containing glucose concentration exceeding 3.8 mM, supporting the authors' hypothesis. The small share of the oxidized gold at lower concentrations is constant and most likely arose during the electrode pre-treatment. The adsorption of H_2O_2 to the components of the model system of Au/TiO_2 and decomposition to 2OH while interaction with surface hydroxyls on TiO_2(100) can provide a low barrier to a surface OOH species, and even water formation [68]. Ishida et al. explored the decomposition of H_2O_2 with the use of different AuNPs' sizes and formation of active oxide species [69]. Studies show that gold nanoparticles can interact with O_2 and be used for catalysis at room temperature [70,71].

The proposed mechanism of glucose interaction with GOx-functionalized Au-TiND electrode is summarized in **Fig. 7**. According to the previously provided explanation, the first concentration range (0 – 1.9 mM) is characterized by the saturation of the outer active centers within the GOx-functionalized film, producing H_2O_2, which then takes part in $FADH_2$

conversion to FAD. The process mentioned above is assisted with the increase of the film resistance, but the global change in electrode homogeneity is negligible due to the small-sized glucose-saturated areas. The possible evolution of analyzed impedance is restricted to outer functionalization coating.

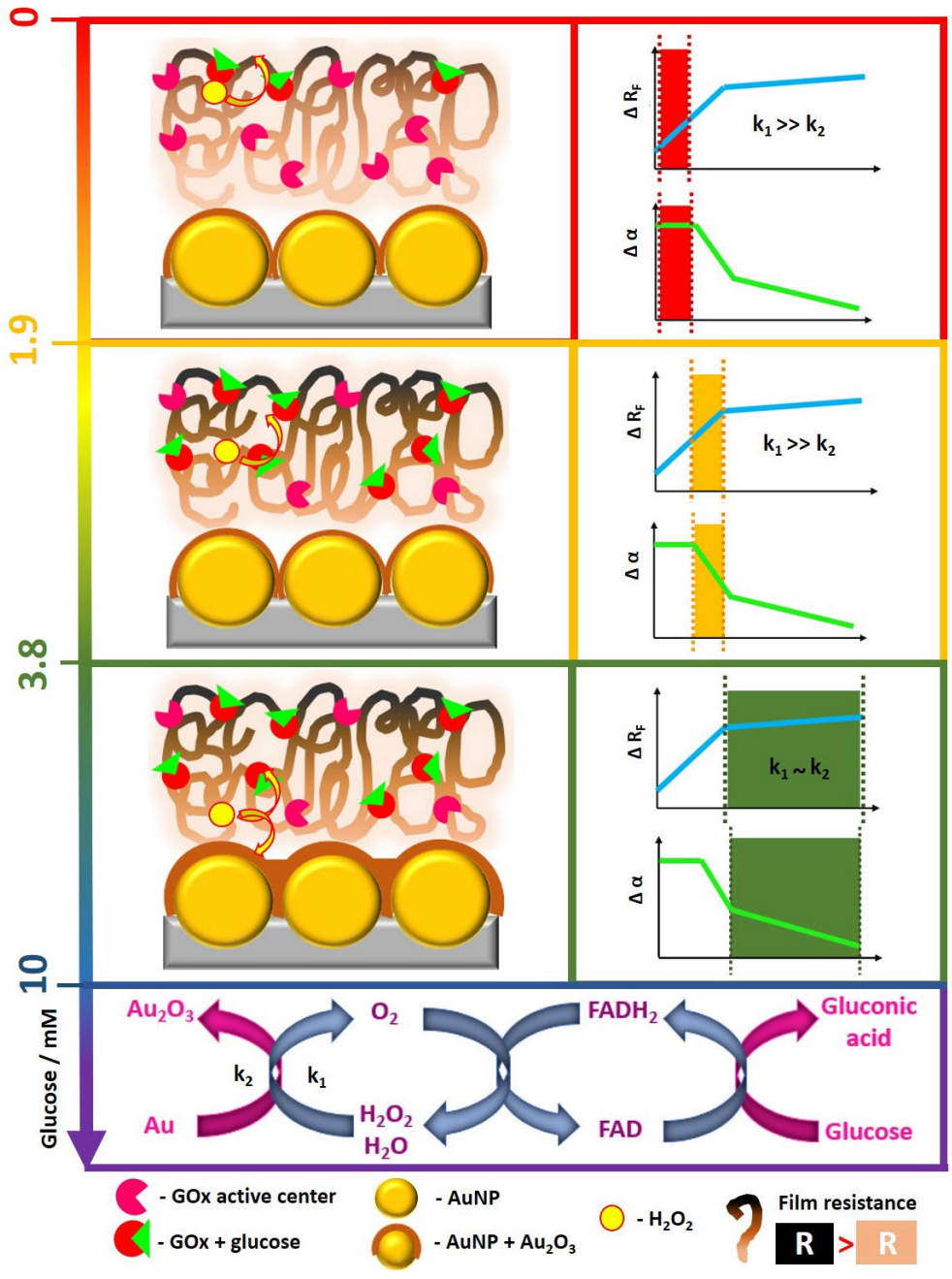

Fig. 7. Schematic representation of the kinetic changes occurring at the GO-functionalized Au-TiND electrode during glucose injection at a constant rate.

The more glucose is injected (range 1.9 – 3.8 mM), the more complex changes are observed. The electrode homogeneity significantly decreases, which can be traced primarily by the CPE exponent *α*. Presumably, the electrode is now characterized by surface and normal

distribution of the time constants, and glucose can saturate inner functionalization layers. Notably, the derivative of the solution resistance and functionalized film resistance changes remain the same as they were in the first stage.

In the last analyzed glucose concentration range (3.8 – 10 mM), at least some of the active centers in the whole volume of GOx-functionalized layer are saturated, leading to the production of H_2O_2 species directly in the vicinity of gold nanoparticles substrate. As a consequence, no further ΔR_F changes are observed. Since all the active centers are saturated, the H_2O_2 produced in the nearest vicinity of the electrode surface leads to gold oxidation. The process proceeds competitively to eq. (6). At this concentration range, the parallel resistance is not solely bound to the functionalized film resistance but also the charge transfer resistance of gold oxidation, as discussed during EEC selection. Initiation of the electron transfer process results in a subsequent drop of parallel resistance [7,15]. Above 10 mM concentration, all active centers in the enzyme are saturated by the glucose molecules, and the overall process is inhibited, being dependent on the FAD to $FADH_2$ transformation rate.

4. Conclusions

We have proposed a new protocol to explore the complex, multi-step electrochemical response of nanotextured surfaces. The studies allowed tracking glucose oxidation at GOx-functionalized AuNPs. Dynamic impedimetric measurements in the galvanostatic mode guaranteed a non-destructive and reproducible environment, partially omitting the electrode's initial state's lack of knowledge. Moreover, the g-DEIS allows for an accurate and easy Michaelis-Menten constant determination, which was found to be 2.45 mM.

The novel approach with g-DEIS allows to observe subtle variations in the kinetics of the analyzed process due to below-summarized interactions: i) the decrease of GOx activity by oxygen dissolved in the electrolyte, presumably due to formation of semiconductive TiO_2 thin film; ii) change in the electrode homogeneity due to GOx active centers saturation at glucose concentrations exceeding 3.8 mM; iii) irreversible AuNP oxidation by hydrogen peroxide produced during GOx($FADH_2$) transformation in the nearest vicinity of the nanotextured electrode surface. The gold oxidation process further affects electrode homogeneity and, in consequence - kinetics. This multi-step behavior was first confirmed by g-DEIS measurements and positively verified using XPS and CV studies. The results indicate that the proposed approach's unique features could significantly spread further application of targetable biosensors for real-time diagnostics. At the same time, the information obtained with g-DEIS

should be considered to prepare calibration curves upon analyte dosing when the electrode's performance is examined.

Acknowledgements

This work is financially supported by The National Centre for Research and Development via grant no LIDER/2/0003/L-8/16/NCBR/2017, The National Science Centre via SONATA grant no 2015/17/ST5/02571 and The Ministry of Science and Higher Education of Poland from the budget funds in period 2016-2019 under Iuventus Plus project IP2015 067574.

5. References

[1] R.A. Dorledo de Faria, H. Iden, L.G.D. Heneine, T. Matencio, Y. Messaddeq, Non-Enzymatic Impedimetric Sensor Based on 3-Aminophenylboronic Acid Functionalized Screen-Printed Carbon Electrode for Highly Sensitive Glucose Detection, Sensors. 19 (2019) 1686. https://doi.org/10.3390/s19071686.

[2] T.L. Adamson, F.A. Eusebio, C.B. Cook, J.T. LaBelle, The promise of electrochemical impedance spectroscopy as novel technology for the management of patients with diabetes mellitus, The Analyst. 137 (2012) 4179. https://doi.org/10.1039/c2an35645g.

[3] A. Ruiz-Vargas, A. Ivorra, J.W. Arkwright, Design, Construction and Validation of an Electrical Impedance Probe with Contact Force and Temperature Sensors Suitable for in-vivo Measurements, Sci. Rep. 8 (2018) 14818. https://doi.org/10.1038/s41598-018-33221-4.

[4] P. Niedzialkowski, P. Slepski, J. Wysocka, J. Chamier-Cieminska, L. Burczyk, M. Sobaszek, A. Wcislo, T. Ossowski, R. Bogdanowicz, J. Ryl, Multisine impedimetric probing of biocatalytic reactions for label-free detection of DEFB1 gene: How to verify that your dog is not human?, Sens. Actuators B Chem. 323 (2020) 128664. https://doi.org/10.1016/j.snb.2020.128664.

[5] M. Carminati, Advances in High-Resolution Microscale Impedance Sensors, J. Sens. 2017 (2017) 1–15. https://doi.org/10.1155/2017/7638389.

[6] K. Darowicki, Theoretical description of the measuring method of instantaneous impedance spectra, J. Electroanal. Chem. 486 (2000) 101–105. https://doi.org/10.1016/S0022-0728(00)00110-8.

[7] K. Darowicki, P. Ślepski, Dynamic electrochemical impedance spectroscopy of the first order electrode reaction, J. Electroanal. Chem. 547 (2003) 1–8. https://doi.org/10.1016/S0022-0728(03)00154-2.

[8] J. Orlikowski, J. Ryl, M. Jarzynka, S. Krakowiak, K. Darowicki, Instantaneous Impedance Monitoring of Aluminum Alloy 7075 Corrosion in Borate Buffer with Admixed Chloride Ions, CORROSION. 71 (2015) 828–838. https://doi.org/10.5006/1546.

[9] S. Krakowiak, K. Darowicki, Electrochemical and acoustic emission studies of aluminum pitting corrosion, J. Solid State Electrochem. 13 (2009) 1653–1657. https://doi.org/10.1007/s10008-008-0759-0.

[10] H. Gerengi, H. Goksu, P. Slepski, The inhibition effect of mad Honey on corrosion of 2007-type aluminium alloy in 3.5% NaCl solution, Mater. Res. 17 (2013) 255–264. https://doi.org/10.1590/S1516-14392013005000174.

[11] M.M. Solomon, H. Gerengi, T. Kaya, S.A. Umoren, Enhanced corrosion inhibition effect of chitosan for St37 in 15% H 2 SO 4 environment by silver nanoparticles, Int. J. Biol. Macromol. 104 (2017) 638–649. https://doi.org/10.1016/j.ijbiomac.2017.06.072.

[12] S. Nagarajan, N. Rajendran, Crevice corrosion behaviour of superaustenitic stainless steels: Dynamic electrochemical impedance spectroscopy and atomic force microscopy studies, Corros. Sci. 51 (2009) 217–224. https://doi.org/10.1016/j.corsci.2008.11.008.
[13] X. Zhu, L. Fernández Macía, J. Jaguemont, J. de Hoog, A. Nikolian, N. Omar, A. Hubin, Electrochemical impedance study of commercial LiNi0.80Co0.15Al0.05O2 electrodes as a function of state of charge and aging, Electrochimica Acta. 287 (2018) 10–20. https://doi.org/10.1016/j.electacta.2018.08.054.
[14] P. Slepski, K. Darowicki, E. Janicka, G. Lentka, A complete impedance analysis of electrochemical cells used as energy sources, J. Solid State Electrochem. 16 (2012) 3539–3549. https://doi.org/10.1007/s10008-012-1825-1.
[15] P. Slepski, K. Darowicki, K. Andrearczyk, On-line measurement of cell impedance during charging and discharging process, J. Electroanal. Chem. 633 (2009) 121–126. https://doi.org/10.1016/j.jelechem.2009.05.002.
[16] J. Ryl, J. Wysocka, P. Slepski, K. Darowicki, Instantaneous impedance monitoring of synergistic effect between cavitation erosion and corrosion processes, Electrochimica Acta. 203 (2016) 388–395. https://doi.org/10.1016/j.electacta.2016.01.216.
[17] K. Darowicki, J. Orlikowski, Impedance analysis of Portevin-Le Chatelier effect on aluminium alloy, Electrochimica Acta. 52 (2007) 4043–4052. https://doi.org/10.1016/j.electacta.2006.11.022.
[18] A.S. Bondarenko, Analysis of large experimental datasets in electrochemical impedance spectroscopy, Anal. Chim. Acta. 743 (2012) 41–50. https://doi.org/10.1016/j.aca.2012.06.055.
[19] M. Szociński, K. Darowicki, Performance of zinc-rich coatings evaluated using AFM-based electrical properties imaging, Prog. Org. Coat. 96 (2016) 58–64. https://doi.org/10.1016/j.porgcoat.2016.02.006.
[20] A. Zieliński, K. Darowicki, Implementation and Validation of Multisinusoidal, Fast Impedance Measurements in Atomic Force Microscope Contact Mode, Microsc. Microanal. 20 (2014) 974–981. https://doi.org/10.1017/S1431927614000531.
[21] K. Darowicki, J. Kawula, Impedance characterization of the process of polyaniline first redox transformation after aniline electropolymerization, Electrochimica Acta. 49 (2004) 4829–4839. https://doi.org/10.1016/j.electacta.2004.05.035.
[22] K. Cysewska, L.F. Macía, P. Jasiński, A. Hubin, In-situ odd random phase electrochemical impedance spectroscopy study on the electropolymerization of pyrrole on iron in the presence of sodium salicylate – The influence of the monomer concentration, Electrochimica Acta. 290 (2018) 520–532. https://doi.org/10.1016/j.electacta.2018.09.069.
[23] B. Rikhari, S. Pugal Mani, N. Rajendran, Electrochemical behavior of polypyrrole/chitosan composite coating on Ti metal for biomedical applications, Carbohydr. Polym. 189 (2018) 126–137. https://doi.org/10.1016/j.carbpol.2018.01.042.
[24] J. Ryl, J. Wysocka, M. Cieslik, H. Gerengi, T. Ossowski, S. Krakowiak, P. Niedzialkowski, Understanding the origin of high corrosion inhibition efficiency of bee products towards aluminium alloys in alkaline environments, Electrochimica Acta. 304 (2019) 263–274. https://doi.org/10.1016/j.electacta.2019.03.012.
[25] J. Wysocka, M. Cieslik, S. Krakowiak, J. Ryl, Carboxylic acids as efficient corrosion inhibitors of aluminium alloys in alkaline media, Electrochimica Acta. 289 (2018) 175–192. https://doi.org/10.1016/j.electacta.2018.08.070.
[26] A.S. Bondarenko, I.E.L. Stephens, H.A. Hansen, F.J. Pérez-Alonso, V. Tripkovic, T.P. Johansson, J. Rossmeisl, J.K. Nørskov, I. Chorkendorff, The Pt(111)/Electrolyte Interface under Oxygen Reduction Reaction Conditions: An Electrochemical Impedance Spectroscopy Study, Langmuir. 27 (2011) 2058–2066. https://doi.org/10.1021/la1042475.
[27] A. Afzal, A. Mujahid, R. Schirhagl, S. Bajwa, U. Latif, S. Feroz, Gravimetric Viral Diagnostics: QCM Based Biosensors for Early Detection of Viruses, Chemosensors. 5 (2017) 7. https://doi.org/10.3390/chemosensors5010007.
[28] M. Procek, A. Stolarczyk, T. Pustelny, E. Maciak, A Study of a QCM Sensor Based on TiO2 Nanostructures for the Detection of NO2 and Explosives Vapours in Air, Sensors. 15 (2015) 9563–9581. https://doi.org/10.3390/s150409563.

[29] J.M. Smulko, K. Darowicki, A. Zielinski, On Electrochemical Noise Analysis for Monitoring of Uniform Corrosion Rate, IEEE Trans. Instrum. Meas. 56 (2007) 2018–2023. https://doi.org/10.1109/TIM.2007.895624.
[30] H. An, T. Habib, S. Shah, H. Gao, A. Patel, I. Echols, X. Zhao, M. Radovic, M.J. Green, J.L. Lutkenhaus, Water Sorption in MXene/Polyelectrolyte Multilayers for Ultrafast Humidity Sensing, ACS Appl. Nano Mater. 2 (2019) 948–955. https://doi.org/10.1021/acsanm.8b02265.
[31] A. Arif Topçu, E. Özgür, F. Yılmaz, N. Bereli, A. Denizli, Real time monitoring and label free creatinine detection with artificial receptors, Mater. Sci. Eng. B. 244 (2019) 6–11. https://doi.org/10.1016/j.mseb.2019.04.018.
[32] J. Ryl, K. Darowicki, P. Slepski, Evaluation of cavitation erosion–corrosion degradation of mild steel by means of dynamic impedance spectroscopy in galvanostatic mode, Corros. Sci. 53 (2011) 1873–1879. https://doi.org/10.1016/j.corsci.2011.02.004.
[33] H. Gerengi, K. Darowicki, P. Slepski, G. Bereket, J. Ryl, Investigation effect of benzotriazole on the corrosion of brass-MM55 alloy in artificial seawater by dynamic EIS, J. Solid State Electrochem. 14 (2010) 897–902. https://doi.org/10.1007/s10008-009-0923-1.
[34] E. Svanidze, T. Besara, M.F. Ozaydin, C.S. Tiwary, J.K. Wang, S. Radhakrishnan, S. Mani, Y. Xin, K. Han, H. Liang, T. Siegrist, P.M. Ajayan, E. Morosan, High hardness in the biocompatible intermetallic compound β-Ti $_3$ Au, Sci. Adv. 2 (2016) e1600319. https://doi.org/10.1126/sciadv.1600319.
[35] W. Lipińska, K. Siuzdak, J. Ryl, P. Barski, G. Śliwiński, K. Grochowska, The optimization of enzyme immobilization at Au-Ti nanotextured platform and its impact onto the response towards glucose in neutral media, Mater. Res. Express. 6 (2019) 1150e3. https://doi.org/10.1088/2053-1591/ab4fab.
[36] F.N. Crespilho, M. Emilia Ghica, M. Florescu, F.C. Nart, O.N. Oliveira, C.M.A. Brett, A strategy for enzyme immobilization on layer-by-layer dendrimer–gold nanoparticle electrocatalytic membrane incorporating redox mediator, Electrochem. Commun. 8 (2006) 1665–1670. https://doi.org/10.1016/j.elecom.2006.07.032.
[37] Z. Li, F. Gao, Z. Gu, Vertically aligned Pt nanowire array/Au nanoparticle hybrid structure as highly sensitive amperometric biosensors, Sens. Actuators B Chem. 243 (2017) 1092–1101. https://doi.org/10.1016/j.snb.2016.12.033.
[38] K. Grochowska, M. Szkoda, J. Karczewski, G. Śliwiński, K. Siuzdak, Ordered titanium templates functionalized by gold films for biosensing applications – Towards non-enzymatic glucose detection, Talanta. 166 (2017) 207–214. https://doi.org/10.1016/j.talanta.2017.01.075.
[39] K. Grochowska, K. Siuzdak, Ł. Macewicz, F. Skiba, M. Szkoda, J. Karczewski, Ł. Burczyk, G. Śliwiński, Nanostructuring of thin Au films deposited on ordered Ti templates for applications in SERS, Appl. Surf. Sci. 418 (2017) 472–480. https://doi.org/10.1016/j.apsusc.2016.12.163.
[40] K. Darowicki, K. Andrearczyk, P. Slepski, A. Sierczynska, G. Lota, K. Fic, K. Lota, Determination of Pseudocapacitance Changes of Nickel Oxide NiO Electrode with the Use of Dynamic Electrochemical Impedance Spectroscopy, Int. J. Electrochem. Sci. 9 (2014) 1702–1714.
[41] V. Ganesh, S. Pitchumani, V. Lakshminarayanan, New symmetric and asymmetric supercapacitors based on high surface area porous nickel and activated carbon, J. Power Sources. 158 (2006) 1523–1532. https://doi.org/10.1016/j.jpowsour.2005.10.090.
[42] R. Golshaei, T. Karazehir, S.M. Ghoreishi, M. Ates, A.S. Sarac, Glucose oxidase immobilization onto Au/poly[anthranilic acid-co-3-carboxy-N-(2-thenylidene)aniline]/PVAc electrospun nanofibers, Polym. Bull. 74 (2017) 1493–1517. https://doi.org/10.1007/s00289-016-1786-0.
[43] K.-Y. Hwa, B. Subramani, Immobilization of Glucose Oxidase on Gold Surface for Applications in Implantable Biosensors, J. Med. Bioeng. 4 (2015) 297–301. https://doi.org/10.12720/jomb.4.4.297-301.
[44] M.M. Barsan, T.A. Enache, N. Preda, G. Stan, N.G. Apostol, E. Matei, A. Kuncser, V.C. Diculescu, Direct Immobilization of Biomolecules through Magnetic Forces on Ni Electrodes via Ni Nanoparticles: Applications in Electrochemical Biosensors, ACS Appl. Mater. Interfaces. 11 (2019) 19867–19877. https://doi.org/10.1021/acsami.9b04990.
[45] B. Hirschorn, M.E. Orazem, B. Tribollet, V. Vivier, I. Frateur, M. Musiani, Determination of effective capacitance and film thickness from constant-phase-element parameters, Electrochimica Acta. 55 (2010) 6218–6227. https://doi.org/10.1016/j.electacta.2009.10.065.

[46] K.-Y. Hwa, B. Subramani, Immobilization of Glucose Oxidase on Gold Surface for Applications in Implantable Biosensors, J. Med. Bioeng. 4 (2015) 297–301. https://doi.org/10.12720/jomb.4.4.297-301.
[47] M. Huang, J.B. Henry, B.B. Berkes, A. Maljusch, W. Schuhmann, A.S. Bondarenko, Towards a detailed in situ characterization of non-stationary electrocatalytic systems, The Analyst. 137 (2012) 631–640. https://doi.org/10.1039/C1AN15671C.
[48] L. Wang, J. Bai, X. Bo, X. Zhang, L. Guo, A novel glucose sensor based on ordered mesoporous carbon–Au nanoparticles nanocomposites, Talanta. 83 (2011) 1386–1391. https://doi.org/10.1016/j.talanta.2010.11.022.
[49] T.J. Davies, C.E. Banks, R.G. Compton, Voltammetry at spatially heterogeneous electrodes, J. Solid State Electrochem. 9 (2005) 797–808. https://doi.org/10.1007/s10008-005-0699-x.
[50] T.J. Davies, R.R. Moore, C.E. Banks, R.G. Compton, The cyclic voltammetric response of electrochemically heterogeneous surfaces, J. Electroanal. Chem. 574 (2004) 123–152. https://doi.org/10.1016/j.jelechem.2004.07.031.
[51] B.A. Brookes, T.J. Davies, A.C. Fisher, R.G. Evans, S.J. Wilkins, K. Yunus, J.D. Wadhawan, R.G. Compton, Computational and Experimental Study of the Cyclic Voltammetry Response of Partially Blocked Electrodes. Part 1. Nonoverlapping, Uniformly Distributed Blocking Systems, J. Phys. Chem. B. 107 (2003) 1616–1627. https://doi.org/10.1021/jp021810v.
[52] X. Liao, V.G.S. Raghavan, V. Meda, V.A. Yaylayan, Dielectric Properties of Supersaturated α-D-Glucose Aqueous Solutions at 2450 MHz, J. Microw. Power Electromagn. Energy. 36 (2001) 131–138. https://doi.org/10.1080/08327823.2001.11688455.
[53] J. Lović, S. Stevanović, N.D. Nikolić, S. Petrović, D. Vuković, N. Prlainović, D. Mijin, M. Avramov Ivić, Glucose Sensing Using Glucose Oxidase-Glutaraldehyde- Cysteine Modified Gold Electrode, Int. J. Electrochem. Sci. 12 (2017) 5806–5817. https://doi.org/10.20964/2017.07.65.
[54] S.B. Bankar, M.V. Bule, R.S. Singhal, L. Ananthanarayan, Glucose oxidase — An overview, Biotechnol. Adv. 27 (2009) 489–501. https://doi.org/10.1016/j.biotechadv.2009.04.003.
[55] Y. Lin, M. Zhao, Y. Guo, X. Ma, F. Luo, L. Guo, B. Qiu, G. Chen, Z. Lin, Multicolor Colormetric Biosensor for the Determination of Glucose based on the Etching of Gold Nanorods, Sci. Rep. 6 (2016) 37879. https://doi.org/10.1038/srep37879.
[56] M.J. Danilich, D. Gervasio, R.E. Marchant, Activity of free and immobilized glucose oxidase: An electrochemical study, Ann. Biomed. Eng. 21 (1993) 655–668. https://doi.org/10.1007/BF02368645.
[57] K.E. Toghill, R.G. Compton, Electrochemical non-enzymatic glucose sensors: a perspective and an evaluation, Int. J. Electrochem. Sci. 5 (2010) 1246–1301.
[58] X. Zeng, Y. Zhang, X. Du, Y. Li, W. Tang, A highly sensitive glucose sensor based on a gold nanoparticles/polyaniline/multi-walled carbon nanotubes composite modified glassy carbon electrode, New J. Chem. 42 (2018) 11944–11953. https://doi.org/10.1039/C7NJ04327A.
[59] V. Buk, M.E. Pemble, K. Twomey, Fabrication and evaluation of a carbon quantum dot/gold nanoparticle nanohybrid material integrated onto planar micro gold electrodes for potential bioelectrochemical sensing applications, Electrochimica Acta. 293 (2019) 307–317. https://doi.org/10.1016/j.electacta.2018.10.038.
[60] T.C. Gokoglan, M. Kesik, S. Soylemez, R. Yuksel, H.E. Unalan, L. Toppare, Paper Based Glucose Biosensor Using Graphene Modified with a Conducting Polymer and Gold Nanoparticles, J. Electrochem. Soc. 164 (2017) G59–G64. https://doi.org/10.1149/2.0791706jes.
[61] B.M. Dixon, J.P. Lowry, R.D. O'Neill, Characterization in vitro and in vivo of the oxygen dependence of an enzyme/polymer biosensor for monitoring brain glucose, J. Neurosci. Methods. 119 (2002) 135–142. https://doi.org/10.1016/S0165-0270(02)00170-X.
[62] P. Naderi Asrami, P. Aberoomand Azar, M. Saber Tehrani, S.A. Mozaffari, Glucose Oxidase/Nano-ZnO/Thin Film Deposit FTO as an Innovative Clinical Transducer: A Sensitive Glucose Biosensor, Front. Chem. 8 (2020) 503. https://doi.org/10.3389/fchem.2020.00503.
[63] P. Khandelwal, A. Alam, A. Choksi, S. Chattopadhyay, P. Poddar, Retention of Anticancer Activity of Curcumin after Conjugation with Fluorescent Gold Quantum Clusters: An in Vitro and in Vivo Xenograft Study, ACS Omega. 3 (2018) 4776–4785. https://doi.org/10.1021/acsomega.8b00113.

[64] K. Grochowska, J. Ryl, J. Karczewski, G. Śliwiński, A. Cenian, K. Siuzdak, Non-enzymatic flexible glucose sensing platform based on nanostructured TiO2 – Au composite, J. Electroanal. Chem. 837 (2019) 230–239. https://doi.org/10.1016/j.jelechem.2019.02.040.
[65] K. Grochowska, K. Siuzdak, Ł. Macewicz, F. Skiba, M. Szkoda, J. Karczewski, Ł. Burczyk, G. Śliwiński, Nanostructuring of thin Au films deposited on ordered Ti templates for applications in SERS, Appl. Surf. Sci. 418 (2017) 472–480. https://doi.org/10.1016/j.apsusc.2016.12.163.
[66] K. Juodkazis, XPS studies on the gold oxide surface layer formation, Electrochem. Commun. 2 (2000) 503–507. https://doi.org/10.1016/S1388-2481(00)00069-2.
[67] M. Tchaplyguine, M.-H. Mikkelä, C. Zhang, T. Andersson, O. Björneholm, Gold Oxide Nanoparticles with Variable Gold Oxidation State, J. Phys. Chem. C. 119 (2015) 8937–8943. https://doi.org/10.1021/acs.jpcc.5b00811.
[68] A. Thetford, G.J. Hutchings, S.H. Taylor, D.J. Willock, The decomposition of H_2O_2 over the components of Au/TiO_2 catalysts, Proc. R. Soc. Math. Phys. Eng. Sci. 467 (2011) 1885–1899. https://doi.org/10.1098/rspa.2010.0561.
[69] T. Ishida, K. Kuroda, N. Kinoshita, W. Minagawa, M. Haruta, Direct deposition of gold nanoparticles onto polymer beads and glucose oxidation with H2O2, J. Colloid Interface Sci. 323 (2008) 105–111. https://doi.org/10.1016/j.jcis.2008.02.046.
[70] P. Jiang, S. Porsgaard, F. Borondics, M. Köber, A. Caballero, H. Bluhm, F. Besenbacher, M. Salmeron, Room-Temperature Reaction of Oxygen with Gold: An In situ Ambient-Pressure X-ray Photoelectron Spectroscopy Investigation, J. Am. Chem. Soc. 132 (2010) 2858–2859. https://doi.org/10.1021/ja909987j.
[71] N. Lopez, J.K. Nørskov, Catalytic CO Oxidation by a Gold Nanoparticle: A Density Functional Study, J. Am. Chem. Soc. 124 (2002) 11262–11263. https://doi.org/10.1021/ja026998a.

Supplementary Information

for

Exploring Multi-step Glucose Oxidation Kinetics at GOx-functionalized Nanotextured Gold Surfaces with Differential Impedimetric Technique

Wiktoria Lipińska[1], Jacek Ryl[2,3*], Paweł Ślepski[2], Katarzyna Siuzdak[1] and Katarzyna Grochowska[1,*]

[1]Centre for Plasma and Laser Engineering, The Szewalski Institute of Fluid-Flow Machinery, Polish Academy of Sciences, Fiszera 14, 80-231 Gdańsk, Poland

[2]Department of Electrochemistry, Corrosion and Material Engineering, Gdańsk University of Technology, Narutowicza 11/12, 80-233 Gdańsk, Poland

[3]Advanced Materials Center, Gdańsk University of Technology, Narutowicza 11/12, 80-233 Gdańsk, Poland

S1. Estimation of the impedimetric results with different electric equivalent circuits

Although within the manuscript we have chosen $R_S(CPE\text{-}R_F)$ EEC, other equivalent circuits were also taken into consideration during our studies. In particular we have considered the utilization of Warburg element to simulate the diffusion resistance, which based on the literature survey [1,2] .

First, we have applied the simple Randles circuit expanded only with Warburg impedance in series with GOx-functionalized film resistance: $R_S(C(R_FW))$. This circuit does not take into consideration the surface heterogeneity, originating from complex and nanotextured GOx/Au-TiND electrode structure as well as saturation of enzyme active centres by glucose. The results of impedance analysis with $R_S(C(R_FW))$ EEC are shown on Fig. S1.

Authors have chosen exactly the same data, which served to present Figs. 2d, 3, 4 and 5 to provide easy illustration how EEC selection affects not only the values but also the distribution of obtained fitting quality. The functionalized film resistance R_F (Fig. S1a) is characterized both with unreasonably low values as well as very high spread, ranging 9 orders of magnitude. The lack of continuity of this parameter versus time and glucose concentration should be considered the decisive factor affecting EEC selection. Such high fluctuation in R_F are inexplicable, which concludes that $R_S(C(R_FW))$ is not capable to provide projection of real physical parameters.

On the other hand, both values and trend of changes in the capacitance (Fig. S1b) are nearly mirroring the C_{EFF} data, based on Hirschorn model and presented on Fig. 5. It should be noted that the spread of the

obtained data is slightly higher in this case. Warburg coefficient *W* obtained based on $R_S(C(R_FW))$ EEC show similar discrepancy, with multi-step behaviour somehow correlated with glucose concentration changes as reported within the manuscript.

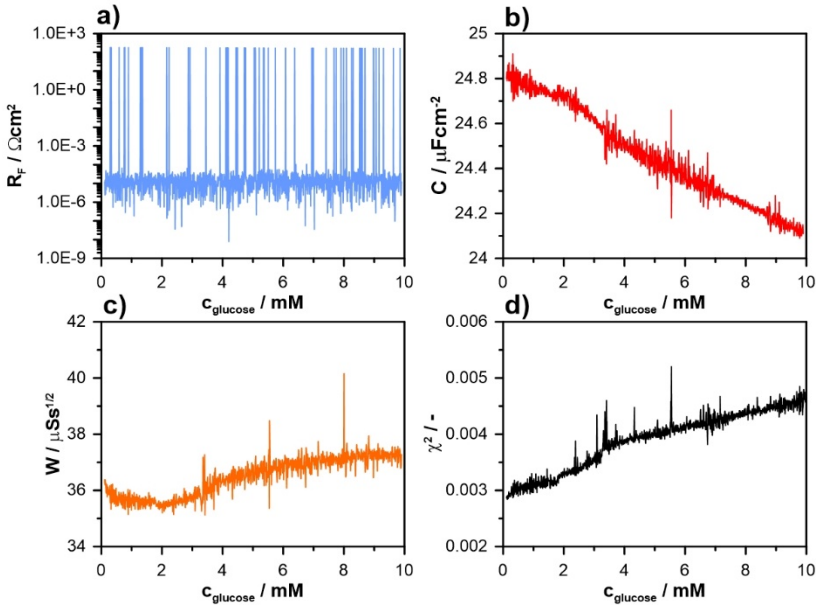

Fig. S1. The results of instantaneous impedance data fitting calculated with $R_S(C(R_FW))$ EEC: a) R_F, b) C, c) W and d) χ^2-distribution. The data were obtained with g-DEIS as a function of injected glucose concentration changes $c_{glucose}$.

However, the value of Warburg coefficient should be dropping with the increase of glucose concentration. Warburg impedance Z_W is a special case of constant phase element CPE for $\alpha = ½$ (see eqs. (1) and (S1)), which in authors opinion leads to a significant dependence between Z_W, capacitance dispersion and increase in electrochemical heterogeneity of the electrode. The Warburg coefficient W may be described using eq. (S2).

$$Z_W = \frac{jW}{\sqrt{\omega}} \tag{S1}$$

$$W = \frac{RT}{An^2F^2\theta C\sqrt{2D}} \tag{S2}$$

where R and F are gas and Faraday constants, respectively, T is thermodynamic temperature, n is the valency, A is electrochemically active surface area, θ is the fraction of reduced and oxidized species, C is the concentration of the electrolyte and D is the diffusion coefficient.

Last but not least, the χ^2-distribution is nearly 3x higher for $R_S(C(R_FW))$ in comparison to $R_S(CPER_F)$ EEC. Importantly, the value of χ^2-distribution was increasing over time, which suggests that the equivalent circuit poorly represents changes introduced by glucose addition.

To summarize, while revealing similarities with $R_S(CPE\text{-}R_F)$ EEC, $R_S(C(R_FW))$ is characterized by inexplicable values and spread of functionalized film resistance during the course of measurements as well as

difficult to explain behaviour of Warburg coefficient function, affected by electrode heterogeneity. The level of fit was decreasing throughout the measurement, suggesting that some physical processes were not included.

Since some of the issues with the discussed above circuit derived from disregarding the capacitance dispersion, the next investigated circuit, R_S(CPE(R_FW)), included CPE instead of a capacitance. The results of impedance analysis with following circuit are presented on Fig. S2.

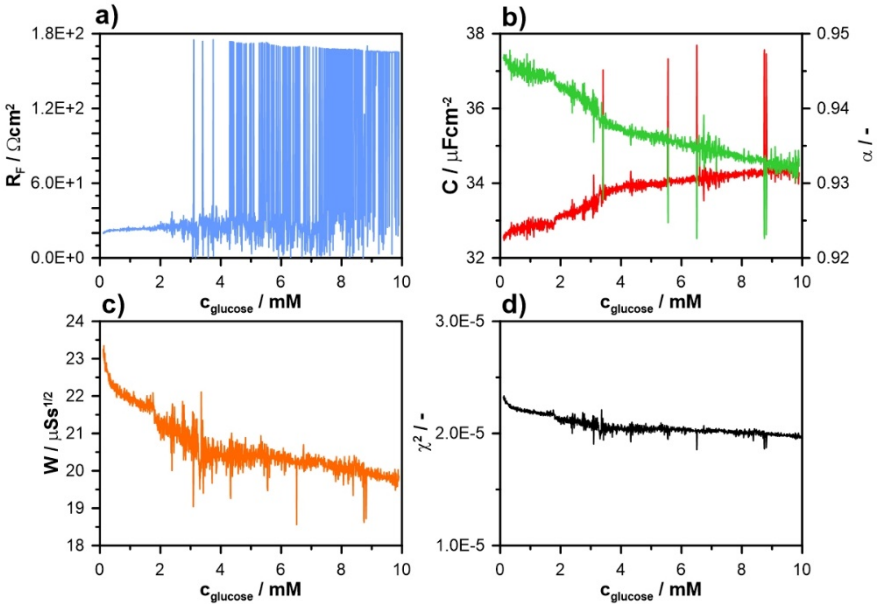

Fig. S2. The results of instantaneous impedance data fitting calculated with R_S(CPE(R_FW)) EEC: a) R_F, b) CPE parameters Q and α, c) W and d) χ^2-distribution. The data were obtained with g-DEIS as a function of injected glucose concentration changes $c_{glucose}$.

The R_S(CPE(R_FW)) EEC had similar difficulties in representation of the parallel resistance changes, in particular in concentration range exceeding 3.8 mM, where gold oxidation process is initiated. Importantly to note, the behaviour of CPE parameters Q and α reveal a similar dependence as in the case of R_S(CPER_F) function, suggesting that inadequate equivalent circuit selection only to a small extend affects the capacitive parameters. This is an important observation, taking into consideration the development of the capacitance sensors, that base on the impedance measurements.

The better fit of this model was further verified by the expected changes in Warburg coefficient over glucose injection. Its linear drop and inflection at 3.8 mM are in good agreement with eq. (S2), suggesting that the parameter is primarily but not exclusively affected with glucose concentration. One should also note, that the calculated W values were two times smaller in comparison with R_S(C(R_FW)) EEC.

The primary reason behind rejection of the R_S(CPE(R_FW)) EEC from further studies was connected with alarmingly high spread of R_F values. Other calculated parameters were also characterized with higher data discrepancy in comparison to R_S(CPE-R_F), but not large enough to hinder the dynamics of changes in electrical parameters. The χ^2-distribution in this case was nearly two orders of magnitude lower, which derives from greater number of degrees of freedom in the applied model.

Due to the restriction of g-DEIS measurements in low-frequency regime (measurements were carried in the frequency range between 4.5 kHz and 0.3 Hz) we came to a conclusion that the Warburg impedance should not be included in the final EEC selection. The diffusion resistance is typically revealed at frequencies beneath 1 Hz.

It is important to observe another emerging advantages of the g-DEIS measurements in comparison with classical EIS approach. The single numerical values most often provided with EIS studies does not allow for a direct verification if changes of the EEC parameters are physically explicable. χ^2-distribution should not be considered the key parameter when discussing the EEC.

S2. The *i*-to-R_F transformation for the Linewaver-Burg equation

Determination of the Michaelis-Menten constant K_M based on Lineweaver-Burg equation requires the knowledge of the current flowing through the electrode at different glucose concentrations. The current function under polarization conditions is described by the Butler-Volmer formula, eq. (S3).

$$i = i_0 \left\{ exp\left[\frac{(1-\alpha)nFE}{RT}\right] - exp\left[\frac{-\alpha nFE}{RT}\right]\right\} \tag{S3}$$

where i_0 is the exchange current, E is the electrode potential, α is charge transfer coefficient, F, R, T, n have their usual meaning. For low overpotentials (the conditions that match our experiment) eq. (S3) may be simplified by replacing the exponential function with a linear function:

$$e^x \approx 1 + x \tag{S4}$$

and modify the Butler-Volmer formula (S3) to simplified form (S5):

$$i = i_0 \frac{nF}{RT} E \tag{S5}$$

Eq. (S5) describes the current response, which is proportional to the voltage perturbation in the studied system and the inverse of the resistance describing the studied reaction. In the simplified form, eq. (S3) may be written as (S6).

$$i = \frac{B}{R_F} \tag{S6}$$

where B is the voltage proportionality coefficient, characteristic for the studied electrochemical process.

References:

[S1] S.S. Ghoreishizadeh, X. Zhang, S. Sharma, P. Georgiou, Study of Electrochemical Impedance of a Continuous Glucose Monitoring Sensor and its Correlation With Sensor Performance, IEEE Sens. Lett. 2 (2018) 1–4. https://doi.org/10.1109/LSENS.2017.2778248.

[S2] R.A. Dorledo de Faria, H. Iden, L.G.D. Heneine, T. Matencio, Y. Messaddeq, Non-Enzymatic Impedimetric Sensor Based on 3-Aminophenylboronic Acid Functionalized Screen-Printed Carbon Electrode for Highly Sensitive Glucose Detection, Sensors. 19 (2019) 1686. https://doi.org/10.3390/s19071686.